Poly(3-hexylthiophene) Molecular Bottlebrushes via Ring-Opening Metathesis Polymerization: Macromolecular Architecture Enhanced Aggregation

Suk-kyun Ahn,[†] Deanna L. Pickel,*[,†] W. Michael Kochemba,[‖] Jihua Chen,[†] David Uhrig,[†] Juan Pablo Hinestrosa,[†] Jan-Michael Carrillo,[‡] Ming Shao,[†] Changwoo Do,[§] Jamie M. Messman,[†] W. Michael Brown,[‡] Bobby G. Sumpter,[†,⊥] and S. Michael Kilbey, II*[,‖]

[†]Center for Nanophase Materials Sciences, [‡]National Center for Computational Sciences, [§]Biology and Soft Matter Division, and [⊥]Computer Science and Mathematics Division, Oak Ridge National Laboratory, Oak Ridge, Tennessee 37831, United States

[‖]Department of Chemistry and of Chemical and Biomolecular Engineering, University of Tennessee, Knoxville, Tennessee 37996, United States

S *Supporting Information*

ABSTRACT: We report a facile synthetic strategy based on a grafting through approach to prepare well-defined molecular bottlebrushes composed of regioregular poly(3-hexylthiophene) (*rr*-P3HT) as the conjugated polymeric side chain. To this end, the *exo*-norbornenyl-functionalized P3HT macromonomer was synthesized by Kumada catalyst transfer polycondensation (KCTP) followed by postpolymerization modifications, and the resulting conjugated macromonomer was successfully polymerized by ring-opening metathesis polymerization (ROMP) in a controlled manner. The P3HT molecular bottlebrushes display an unprecedented strong physical aggregation upon drying during recovery, as verified by several analyses of the solution and solid states. This remarkable strong aggregation behavior is attributed to a significant enhancement in the number of $\pi-\pi$ interactions between grafted P3HT side chains, brought about due to the bottlebrush architecture. This behavior is qualitatively supported by coarse-grained molecular dynamics simulations.
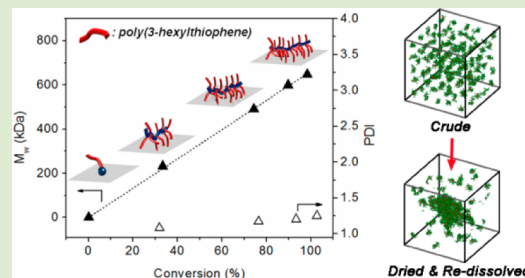
Regioregular poly(3-hexylthiophene) (*rr*-P3HT) is one of the most important conjugated polymers for organic electronic applications including organic photovoltaics (OPVs) and organic field-effect transistors (OFETs). This is due to its excellent hole mobility ($\sim$0.1 cm^2 V^{-1} s^{-1}),[1] solution processability, and ease of synthesis.[2] In particular, versatile chemical modification of P3HT[2a] allows P3HT-based copolymers[2b] and P3HT/nanocrystal hybrids[3] to be created. While the majority of research has concentrated on linear P3HTs, more complex macromolecular architectures provide vast opportunities to tailor morphology and physical properties of the resulting polymers and their hybrids. In this regard, there has been a growing interest in the synthesis of complex P3HT architectures[4] such as grafts,[4a,b] stars,[4c,d] hyperbranched,[4e] and cyclics.[4f]

Molecular bottlebrushes in which polymeric side chains are densely grafted along the polymer backbone are a special class of comb-shaped macromolecules.[5] Bottlebrush polymers in which the length of the backbone is greater than that of the side chain take on an extended backbone conformation, inducing the polymer to adopt a cylindrical shape that results from steric repulsion between the grafts.[5] The unique self-assembly of molecular bottlebrushes in the solution or melt state and their

potential application as nano-, bio-, and photonic materials have drawn considerable attention.[5]

Although numerous examples of molecular bottlebrushes containing insulating polymeric side chains have been reported,[5] those with conjugated polymeric side chains are limited due to the synthetic challenges associated with precise control over chain end functionality. Fréchet and co-workers first demonstrated the synthesis of comb-shaped block copolymers containing P3HT side chains, but the resulting polymers were multimodal by size exclusion chromatography (SEC).[6] More recently, Lin and co-workers reported the synthesis of P3HT copolymer brushes via the grafting to approach.[7] Ethynyl-terminated P3HT was grafted with high efficiency to a poly(4-(azidomethyl)styrene) backbone by Huisgen 1,3-dipolar cycloaddition. To our knowledge, this is the only example of a molecular bottlebrush comprising conjugated polymer side chains.

In this communication we demonstrate the synthesis of well-defined molecular bottlebrushes composed of a poly-(norbornene) backbone and *rr*-P3HT side chains (denoted

PNB-*g*-P3HT). The grafting through approach was used to synthesize P3HT molecular bottlebrushes, allowing copolymers with a high grafting density of well-defined side chains to be made. It should be noted that, while the term "molecular bottlebrush" refers to the case where the backbone length is much greater than the side-chain length, for the sake of convenience we will refer to our materials as molecular bottlebrushes. These P3HT molecular bottlebrushes exhibit unprecedented strong physical aggregation when they are recovered by freeze-drying, as evidenced by characterization in both the solution and the solid states.

The norbornenyl-functionalized P3HT macromonomer was synthesized by the multistep process shown in Scheme 1. First,

Scheme 1. Synthesis of Norbornenyl-Functionalized P3HT Macromonomer (1 → 4) and PNB-*g*-P3HT Molecular Bottlebrushes (4 → 5)
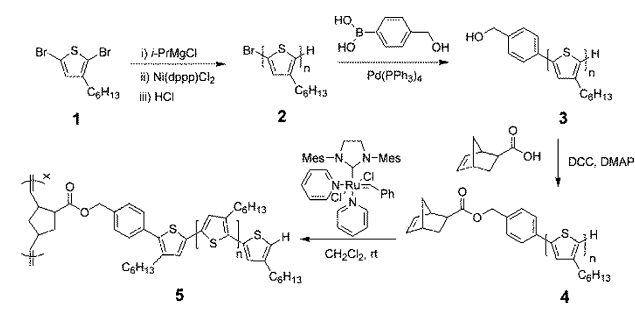
bromine-functionalized P3HT **2** was prepared by Kumada catalyst transfer polycondensation (KCTP) with nickel as the initiator.[8] Under optimized reaction conditions,[8c] including tight control of the stoichiometry and polymerization time, the α-bromine-functionalized P3HT **2** was obtained in high purity (>97%). Next, hydroxy-functionalized P3HT **3** was synthesized by palladium-catalyzed Suzuki coupling using a large excess of 4-hydroxymethylphenylboronic acid relative to **2**.[9] While the major product (>90%) is the desired monohydroxy-functionalized P3HT, several undesired species were also observed by matrix-assisted laser desorption ionization time-of-flight mass spectrometry (MALDI-TOF MS). These impurities were successfully separated from **3** by column chromatography to yield the purified monohydroxy-functionalized P3HT, which we designate as **3a**. Lastly, the *exo*-norbornenyl-functionalized P3HT macromonomer **4** was prepared by *N,N′*-dicyclohexylcarbodiimide (DCC)-promoted coupling. A low molecular weight P3HT macromonomer ($M_{n,Theor} \sim 3.0$ kDa) was synthesized to allow for full characterization of the end groups by a number of methods.

The molecular weights of P3HT **2**, **3**, **3a**, and **4** were characterized by SEC, ^{1}H NMR, and MALDI-TOF MS, and the results are summarized in Table 1. (Also see Figures S1 and S2, Supporting Information.) It is well-known that molecular weight values of P3HT determined by SEC relative to PS standards are overestimated by a factor of 1.2–2.3[10] due to substantial differences in the hydrodynamic volumes of P3HT and PS in THF. The molecular weights obtained by SEC versus those obtained by ^{1}H NMR and MALDI-TOF MS for the end-functionalized P3HTs show a similar discrepancy. It should be noted that molecular weights determined by ^{1}H NMR and MALDI-TOF MS are in good agreement when the end-functionality is high (**2**, **3a**, and **4**), while the value deviates substantially when the end-functionality is low (**3**). All of the

Table 1. Characteristics of End-Functionalized P3HTs

entry	$M_{n,NMR}$ (kDa)[a]	$M_{n,MALDI}$ (kDa)[b]	$M_{n,SEC}$ (kDa)[c]	PDI[c]	functionality (%)[b]
2	2.1	1.9	3.3	1.24	97
3	3.0	2.0	3.9	1.14	90
3a[d]	2.1	2.2	3.6	1.05	>99
4	2.3	2.3	3.8	1.04	>99

[a]Determined by ^{1}H NMR end-group analysis. [b]Determined by MALDI-TOF MS analysis. [c]Determined by SEC relative to PS standards using RI detector with THF as eluent. [d]P3HT-(OH/H) after purification by column chromatography.

end-functionalized polymers exhibit narrow polydispersity indices.

End-group analysis was performed by ^{1}H NMR and MALDI-TOF MS after each synthetic step. Due to overlapping chemical shifts caused by the distribution of P3HTs having different end groups, ^{1}H NMR only provides qualitative information with respect to the end-group composition (Figure S1, Supporting Information) and, therefore, MALDI-TOF was a critical tool for definitive identification of the P3HT end groups.[11] The MALDI-TOF MS spectrum for each end-functionalized P3HT is shown in Figure 1. All samples appear monomodal with a
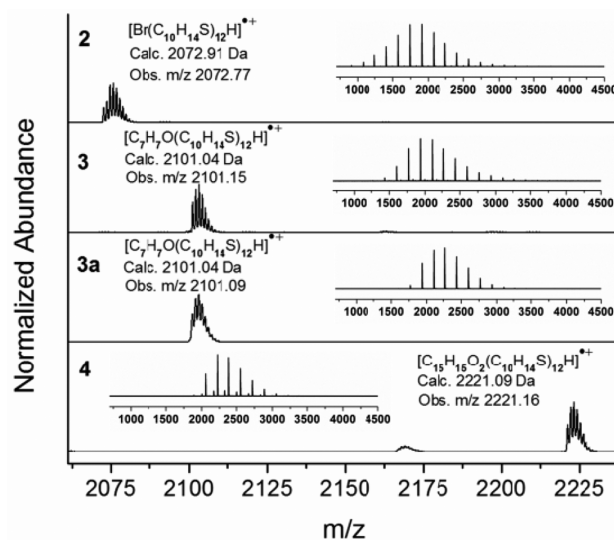

Figure 1. MALDI-TOF mass spectra for end-functionalized P3HTs **2**–**4** as identified in Scheme 1 showing both the entire spectrum (inset) and the region of the 12-mer.

single major distribution, and the calculated monoisotopic masses, which are given in Figure 1, are in excellent agreement with the observed *m/z* of the desired products. In addition, the end-group functionalities of each P3HT were determined by comparing the monoisotopic peak height for each observed distribution. It should be noted that for P3HT **3** a number of byproducts that could be subsequently removed by column chromatography were observed by MALDI-TOF MS (Figure S3, Supporting Information). Also, the small peak observed near *m/z* 2165 in the spectrum of P3HT **4** is likely a metastable peak because it is not observed when the sample is analyzed in linear mode.[12] While limiting side reactions to obtain highly functionalized P3HTs has been extremely challenging,[11] MALDI-TOF MS analysis demonstrates that postpolymerization modifications and stringent purification result in the

successful preparation of norbornenyl-functionalized P3HT with greater than 99% functionality.

ROMP of the P3HT macromonomer **4** was conducted using a modified second-generation Grubbs catalyst[13] as shown in Scheme 1 (from **4** to **5**). Unlike conventional coil-type macromonomers, the reduced solubility and $\pi-\pi$ intermolecular interactions of P3HT may hinder chain growth during the polymerization. Therefore, the polymerizations were conducted at dilute monomer concentrations [5 mM] as compared to conditions typically used for ROMP.[14] During the polymerization, aliquots were withdrawn from the reaction mixture at different time intervals, immediately terminated by ethyl vinyl ether (EVE) and analyzed by SEC. As shown in Figure 2a, the
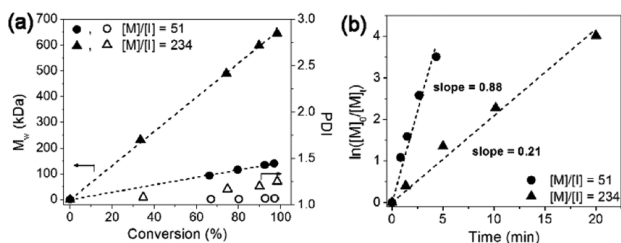
Figure 2. (a) M_w (filled symbols) and PDI (open symbols) as a function of macromonomer conversion and (b) the dependence of $\ln([M]_o/[M]_t)$ on polymerization time.

M_w increases linearly with conversion, and the polydispersity remains low for both [M]/[I] ratios. In addition, growth of the chain follows first-order kinetics, as shown in Figure 2b. These results indicate that despite the high steric demand the norbornenyl-functionalized P3HT macromonomer can be polymerized in a controlled manner, yielding well-defined P3HT molecular bottlebrushes.

Table 2 summarizes the various P3HT molecular bottlebrushes (PNB$_x$-g-P3HT$_y$, where x and y represent the degree of

Table 2. ROMP for P3HT Macromonomer 4

| (PNB$_x$-g-P3HT$_y$)[a]	[M]/[I][b]	$M_{n,theo}$[c] (kDa)	$M_{w,SEC}$[d] (kDa)	PDI[d]	conv. (%)[e]
PNB$_{25}$-g-P3HT$_{12}$	25	57	67	1.09	98
PNB$_{52}$-g-P3HT$_{12}$	52	118	153	1.09	98
PNB$_{100}$-g-P3HT$_{12}$	100	226	288	1.22	97
PNB$_{200}$-g-P3HT$_{12}$	200	396	442	1.43	86

[a]The DPs of the backbone and of the side chain are given by x and y, respectively. [b]Macromonomer to initiator feed ratio. [c]Calculated by ($M_{n,MALDI}$ of macromonomer) × ([M]/[I]) × conversion. [d]Determined by SEC using MALLS detector. [e]Determined by comparing the peak areas of P3HT molecular bottlebrushes and the residual macromonomer from the results of SEC-refractive index (RI) detector.

polymerization (DP) of the backbone and side chain, respectively), prepared by ROMP of the P3HT macromonomer **4**. Due to the living nature of ROMP, polymers of predetermined molecular weight can be prepared by simply varying [M]/[I] as suggested by Figure S4 (Supporting Information). Absolute molecular weights of P3HT molecular bottlebrushes were determined by multiangle laser light scattering (MALLS) using a literature value for the refractive index increment in THF (dn/dc = 0.3 mL/g),[15] and they are in good agreement with calculated molecular weights. Conversion of the macromonomer to P3HT molecular bottlebrushes was high (>86%) in all cases; however, when high [M]/[I] were

used, it is likely that the steric hindrance between the propagating chain end and the macromonomer **4** resulted in lower conversion. Obtaining a high conversion from macromonomer to bottlebrush polymers for high [M]/[I] is an inherent challenge when using the grafting-through method.[5d] The broader polydispersity observed at higher molecular weights may be due to inter- and/or intramolecular chain transfer.[16]

Most interestingly, the P3HT molecular bottlebrushes display an exceptionally strong physical aggregation that was first observed by SEC after the P3HT molecular bottlebrushes were purified by precipitation into methanol, filtration, and freeze-drying from benzene. To highlight this intriguing aggregation behavior, we focus on the aggregation behavior of PNB$_{25}$-g-P3HT$_{12}$ as an example. All other P3HT molecular bottlebrushes exhibited similar aggregation behavior, and the experimental results can be found in the Supporting Information (SI, Figures S5−S8). To distinguish between the polymer solutions, "crude" refers to solutions in THF that were prepared after ROMP but without the freeze-drying step, while "dried" refers to samples that were freeze-dried and then redissolved in THF. (See SI for details.)

SEC traces of the crude and dried solutions of PNB$_{25}$-g-P3HT$_{12}$ in THF are compared in Figure 3a. Signals from the LS
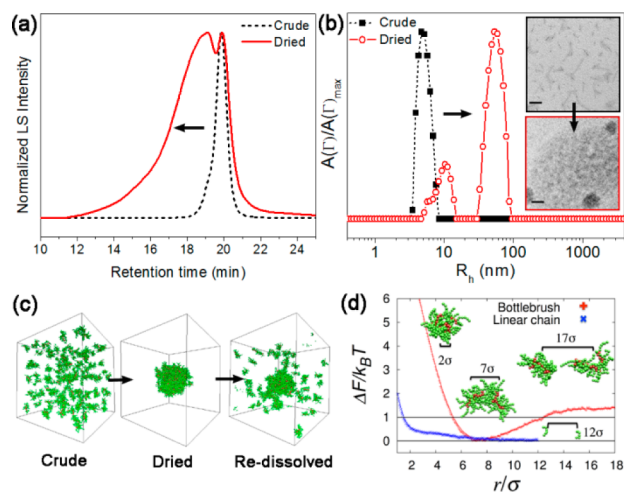
Figure 3. Experimental evidence for physical aggregation of PNB$_{25}$-g-P3HT$_{12}$ upon freeze-drying (a and b) and simulation of the aggregation behavior of P3HT molecular bottlebrushes (c and d). (a) SEC for crude and dried samples in THF (LS detector). (b) Scattering amplitude distribution of crude and dried samples in THF at 25 °C obtained by DLS (inset: TEM images for crude (*top*) and dried (*bottom*), where scale bar is 200 nm). (c) Snapshots for bottlebrush polymers at three different states. (d) Potential of mean force for separating two macromonomers (blue) and two bottlebrush polymers (red). The bottlebrushes and macromoners are modeled using LJ beads with diameter, σ.

detector show that the polydispersity of the crude solution broadens significantly upon freeze-drying. In particular, the appearance of a broad distribution of products emerging at lower retention time indicates the presence of a significant amount of high molecular weight material. We speculate that the appearance of the high molecular weight distribution is likely due to aggregation induced by the freeze-drying process. Moreover, this aggregation proved to be strong: redissolution in THF did not completely disperse the chains. To explore this

behavior, dynamic light scattering (DLS) was performed on crude and dried solutions at ~1 mg/mL in THF. A monomodal distribution (R_h = 6 nm) was observed from the crude solution, while multiple distributions (R_h = 10 and 48 nm) were observed from the dried solution (Figure 3b). The DLS results clearly suggest that the freeze-drying step causes aggregation of P3HT molecular bottlebrushes, which is also reflected in the SEC results. Additionally, UV−vis absorption spectra were collected after diluting these solutions to determine if any additional orderings were induced by the aggregation. However, no changes in the absorption spectra for the crude and dried solutions were observed (Figure S7, SI), suggesting that aggregation occurs in a disordered manner. Similarly, our recent studies of low molecular weight rr-P3HT brushes suggest that intramolecular disorder via conformational defects disrupts cofacial planar stacking of chains that give rise to a vibronic shoulder in the UV−vis spectrum.[17]

This aggregation behavior of P3HT molecular bottlebrushes was further explored using transmission electron microscopy (TEM) and atomic force microscopy (AFM) to probe the thin-film structures, which are related to those adopted by the chains in solution.[15] The same solutions prepared for DLS were drop-cast onto carbon-coated grids for TEM imaging or spun-cast on silicon wafers for AFM studies. TEM images (Figure 3b, inset) show that the P3HT molecular bottlebrushes deposited from the crude product are more dispersed, while aggregated clusters are observed for the dried product. AFM images similarly indicate that P3HT molecular bottlebrushes spun-cast from the crude product are better dispersed as compared to those subjected to drying (Figure S8, SI).

The tendency of P3HTs to aggregate due to their π−π interactions is a well-known behavior.[15] Usually, the aggregated chains can be separated by applying thermal or ultrasonic energy.[15b,18] Han et al. showed using temperature-dependent DLS measurements that loose aggregates formed from rr-P3HT (M_n = 16 kDa) in THF at room temperature were disassembled by increasing the solution temperature to 50 °C.[15b] On the basis of this, we also attempted to break the aggregation of the P3HT molecular bottlebrushes by either holding the dried solution at 50 °C or by using ultrasonication. Solution heating was ineffective, as large aggregates were still present after 3 days and the SEC traces showed only minor changes (Figure S9, SI). However, the aggregates present in the solution were significantly reduced when a strong ultrasonic wave was applied directly to the solution (i.e., tip-sonication). As shown in Figure S10 (SI), SEC traces collected after tip-sonication at different time intervals show (1) a gradual change in the peak molecular weight (M_p) to longer retention times and (2) a narrowing of the molecular weight distribution, both of which clearly suggest that physical aggregation was reduced.

Although the size and relative amount of aggregates were considerably reduced, incomplete dissolution and the energy required for dissociation indicate strong physical aggregation of the P3HT molecular bottlebrushes. This strong aggregation can be attributed to the intrinsic π−π interactions of P3HTs, wherein the number of such contacts is increased by the densely grafted P3HT side chains (i.e., macromolecular architecture enhanced aggregation). To support our hypothesis, coarse-grained molecular dynamics simulations were performed assuming a short-range attractive interaction between side-chain beads (i.e., Lennard-Jones (LJ) potential of ε_{LJ} = 0.43$k_B T$, see SI for simulation details). The simulations show qualitative agreement with the experiments (Figure 3c): P3HT bottle-

brush chains, which are well-dispersed in the crude solution (crude), become aggregated during drying (dried), but the aggregates are only partially redispersed after adding the solvent (redissolved). Indeed, the plot of the "potential of mean force" for separating two bottlebrushes shows a potential well of ~1.5$k_B T$, while such a well is not observed for the linear chains (Figure 3d). This energy well can be attributed to localized side-chain attractions around a backbone. Although we speculate that the strong aggregation of P3HT bottlebrushes is primarily driven by the increase in the number of attractive π−π interactions, other types of noncovalent interactions or physical factors may also contribute to the aggregation. Additional investigations are needed to better resolve this.

In summary, the synthesis of well-defined P3HT molecular bottlebrushes by the grafting-through approach was demonstrated. The norbornenyl-functionalized P3HT macromonomer was prepared by postpolymerization modifications and stringent purification and successfully polymerized in a controlled manner by ROMP in spite of the potentially high steric demand of P3HT side chains. The combination of macromolecular architecture and the inherent intermolecular interactions between the P3HT side chains results in an extremely strong physical aggregation of the bottlebrushes upon drying. Considering the multitude of (macro)monomers that can be polymerized by ROMP, our conjugated macro-monomer has immense potential as a building block to prepare various ROMP-based conjugated copolymers. Moreover, our synthetic approach provides access to architecturally complex P3HT-based materials that may alter self-assembly and properties of optoelectronic devices in useful ways.

■ ASSOCIATED CONTENT

Ⓢ Supporting Information

Experimental procedures, characterizations, synthetic protocols, additional figures, and simulation details. This material is available free of charge via the Internet at http://pubs.acs.org.

■ AUTHOR INFORMATION

Corresponding Author
*E-mail: mkilbey@utk.edu and deannapickel@gmail.com.

Notes
The authors declare no competing financial interest.

■ ACKNOWLEDGMENTS

■ REFERENCES

(1) Sirringhaus, H.; Tessler, N.; Friend, R. H. Science 1998, 280, 1741−1744.
(2) (a) Marrocchi, A.; Lanari, D.; Facchetti, A.; Vaccaro, L. Energy Environ. Sci. 2012, 5, 8457−8474. (b) Stefan, M. C.; Bhatt, M. P.; Sista, P.; Magurudeniya, H. D. Polym. Chem. 2012, 3, 1693−1701.
(3) Zhao, L.; Lin, Z. Adv. Mater. 2012, 24, 4353−4368.

(4) (a) Mougnier, S.-J.; Brochon, C.; Cloutet, E.; Fleury, G.; Cramail, H.; Hadziioannou, G. *Macromol. Rapid Commun.* **2012**, *33*, 703−709. (b) Wang, J.; Lu, C.; Mizobe, T.; Ueda, M.; Chen, W.-C.; Higashihara, T. *Macromolecules* **2013**, *46*, 1783−1793. (c) Yuan, M.; Okamoto, K.; Bronstein, H. A.; Luscombe, C. K. *ACS Macro Lett.* **2012**, *1*, 392−395. (d) Pang, X.; Zhao, L.; Feng, C.; Lin, Z. *Macromolecules* **2011**, *44*, 7176−7183. (e) Okamoto, K.; Housekeeper, J. B.; Michael, F. E.; Luscombe, C. K. *Polym. Chem.* **2013**, *4*, 3499−3506. (f) Coulembier, O.; Deshayes, G.; Surin, M.; De Winter, J.; Boon, F.; Delcourt, C.; Leclere, P.; Lazzaroni, R.; Gerbaux, P.; Dubois, P. *Polym. Chem.* **2013**, *4*, 237−241.

(5) (a) Sheiko, S. S.; Sumerlin, B. S.; Matyjaszewski, K. *Prog. Polym. Sci.* **2008**, *33*, 759−785. (b) Zhang, M.; Müller, A. H. E. *J. Polym. Sci., Part A: Polym. Chem.* **2005**, *43*, 3461−3481. (c) Rzayev, J. *ACS Macro Lett.* **2012**, *1*, 1146−1149. (d) Hadjichristidis, N.; Pitsikalis, M.; Iatrou, H.; Pispas, S. *Macromol. Rapid Commun.* **2003**, *24*, 979−1013.

(6) Sivula, K.; Ball, Z. T.; Watanabe, N.; Fréchet, J. M. J. *Adv. Mater.* **2006**, *18*, 206−210.

(7) Pang, X.; Zhao, L.; Feng, C.; Wu, R.; Ma, H.; Lin, Z. *Polym. Chem.* **2013**, *4*, 2025−2032.

(8) (a) Osaka, I.; McCullough, R. D. *Acc. Chem. Res.* **2008**, *41*, 1202−1214. (b) Kiriy, A.; Senkovskyy, V.; Sommer, M. *Macromol. Rapid Commun.* **2011**, *32*, 1503−1517. (c) Lohwasser, R. H.; Thelakkat, M. *Macromolecules* **2011**, *44*, 3388−3397.

(9) Ho, V.; Boudouris, B. W.; McCulloch, B. L.; Shuttle, C. G.; Burkhardt, M.; Chabinyc, M. L.; Segalman, R. A. *J. Am. Chem. Soc.* **2011**, *133*, 9270−9273.

(10) (a) Liu, J.; Loewe, R. S.; McCullough, R. D. *Macromolecules* **1999**, *32*, 5777−5785. (b) Wong, M.; Hollinger, J.; Kozycz, L. M.; McCormick, T. M.; Lu, Y.; Burns, D. C.; Seferos, D. S. *ACS Macro Lett.* **2012**, *1*, 1266−1269.

(11) (a) Kochemba, W. M.; Kilbey, S. M. II; Pickel, D. L. *J. Polym. Sci., Part A: Polym. Chem.* **2012**, *50*, 2762−2769. (b) Kochemba, W. M.; Pickel, D. L.; Sumpter, B. G.; Chen, J.; Kilbey, S. M., II *Chem. Mater.* **2012**, *24*, 4459−4467. (c) Jeffries-El, M.; Sauvé, G.; McCullough, R. D. *Adv. Mater.* **2004**, *16*, 1017−1019. (d) Jeffries-El, M.; Sauvé, G.; McCullough, R. D. *Macromolecules* **2005**, *38*, 10346−10352.

(12) Quirk, R.; Gomochak, D.; Wesdemiotis, C.; Arnould, M. *J. Polym. Sci., Part A: Polym. Chem.* **2003**, *41*, 947−957.

(13) Love, J. A.; Morgan, J. P.; Trnka, T. M.; Grubbs, R. H. *Angew. Chem., Int. Ed.* **2002**, *41*, 4035−4037.

(14) Xia, Y.; Kornfield, J. A.; Grubbs, R. H. *Macromolecules* **2009**, *42*, 3761−3766.

(15) (a) Huang, Y.; Cheng, H.; Han, C. C. *Macromolecules* **2010**, *43*, 10031−10037. (b) Huang, Y.; Cheng, H.; Han, C. C. *Macromolecules* **2011**, *44*, 5020−5026.

(16) Bielawski, C. W.; Grubbs, R. H. *Prog. Polym. Sci.* **2007**, *32*, 1−29.

(17) Alonzo, J.; Kochemba, W. M.; Pickel, D. L.; Ramanathan, M.; Sun, Z.; Li, D.; Chen, J.; Sumpter, B. G.; Heller, W. T.; Kilbey, S. M., II. *Nanoscale* **2013**, DOI: 10.1039/c3nr02226a.

(18) Kim, B.-G.; Kim, M.-S.; Kim, J. *ACS Nano* **2010**, *4*, 2160−2166.